Theoretical Study on Mechanisms of the Epoxy−Amine Curing Reaction

Jan-Eric Ehlers,[†] Nelson G. Rondan,[‡] Lam K. Huynh,[†] Ha Pham,[‡] Maurice Marks,[‡] and Thanh N. Truong*[,†]

Department of Chemistry, University of Utah, 315 South 1400 East, Room 2020, Salt Lake City, Utah 84112, and The Dow Chemical Company, B-1226, Freeport, Texas 77541

Received February 16, 2007; Revised Manuscript Received March 21, 2007

ABSTRACT: Fundamental understanding of mechanisms of the epoxy−amine curing reaction is crucial for developing new polymer materials. Nearly all experimental studies, to date for elucidating its mechanisms are based on thermometric measurements and thus cannot provide the molecular level details. This study used density functional theory (DFT) methods to examine the mechanism of epoxy−amine poly addition reactions at the molecular level. Different reaction pathways involving both acyclic and cyclic transition state structures were examined for different reaction conditions, namely isolated, self-promoted by amine, catalyzed by alcohol, and in different solvents. The results indicate that the reactions catalyzed by an alcohol dominate the rate over the self-promoted reaction by other amine species and the isolated one in early stages of the conversion. The concerted pathways involving cyclic transition-state complexes are not significant due to their high activation energies. Calculated activation energies are within the experimental uncertainty. In addition, solvent, not steric and electronic effects as suggested earlier, are shown to be responsible for secondary amines to react slower than primary amines.

Introduction

Epoxy compounds have a wide range of technical applications due to their outstanding properties.[1] As all epoxy end-use products require reaction with a curing agent, often an amine, the elucidation of the reaction mechanism is of special interest as indicated by numerous kinetic studies in the last few decades. The general reaction occurs via a nucleophilic attack of the amine nitrogen on the terminal carbon of the epoxy function. The mechanism has been known to be a S_N2-type II, and thus the reaction rate obeys second-order kinetics (cf. Scheme 1).

The reaction may involve both primary and secondary amines[2] as well as hydrogen-bonding catalysts and promoters, which can be shown to have a considerable effect on the activation barrier of the curing reaction.

Narracott,[3] Chapman, Isaacs, and Parker were among the first researchers to suggest a number of several possible reaction pathways that may occur during the curing process and evaluated them according to their importance.[4] The reaction was known to be catalyzed by hydroxyl groups[5] or by catalytic impurity.[6] It was also known that the primary amine reacts twice with an epoxy molecule to form a tertiary amine.[7] Mijovic and co-workers suggested a possible concerted mechanism that involves cyclic hydrogen bond complexes with reactant amine molecules.[8]

These models have been used, refined, or slightly altered or extended to the present time, especially the Horie's model.[9,10] Other approaches were also employed,[11] particularly using kinetic modeling combined with experimental measurements. In such cases, a kinetic model was used involving a set of elementary reactions whose rate parameters were determined by fitting to experimental data from rate equation thermometric measurements conducted with the aid of differential scanning calorimetry (DSC).[12,13] Elucidating the epoxy−amine reaction mechanism, using this approach, has a number of limitations. A major disadvantage is that it cannot provide any information at the molecular level on the mechanism of individual elementary reactions. For example, it cannot address the possibility of cyclic thermolecular transition states with an epoxy and two amine molecules, described in a review by Rozenberg.[14] Cyclic and acyclic transition states of the same stoichiometry cannot be distinguished by thermometric measurements although their reaction pathways for this specific reaction differs considerably; the amine addition via a cyclic transition state is believed to be a concerted one-step process, whereas the acyclic pathway is a stepwise process that occurs via an intermediate. It is a well-accepted fact that the cyclic hydrogen bond complex often stabilizes the transition state, and thus it is considered to be a more favorable pathway in literature.[15,16] This has not been confirmed for the epoxy−amine system, however.

Scheme 1. General Mechanism for Epoxy−Amine Curing.

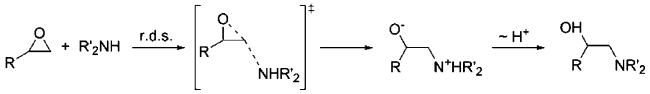

The first step is assumed to be rate determining (rds), and the proton transfer is fast compared to the nucleophilic attack.

Theoretical calculations would be able to bridge the present gaps by providing a fundamental molecular-level understanding of the mechanism of the epoxy−amine curing reaction. Although the current capability of computational methodologies cannot model a realistic poly-addition reaction in the actual condensed phase, examining the potential energy surfaces of reactions in the gas phase and in different solvents using a continuum solvation model will provide valuable insight into the chemistry of this reaction. Interestingly, the employed model reaction together with the accuracy of modern density functional theory (DFT) methods yields results in good agreement with experimental observations. In the present study, we have examined different reaction pathways for the rate-determining step, i.e., the initial conversion using model compounds. Potential energy

* Corresponding author. E-mail: truong@chem.utah.edu.
[†] Department of Chemistry, University of Utah.
[‡] The Dow Chemical Company.

10.1021/ma070423m CCC: $37.00
Published on Web 05/19/2007

curves along these reaction pathways were determined. Equilibrium constants and thermal rate constants for selected dominant pathways were also calculated for comparisons with experimental observation.

Computational Details

All electronic structure calculations were carried out using the Gaussian 03 program package.[17] A hybrid nonlocal density functional theory B3LYP level of theory[18] with the 6-31G(d,p) basis set has been used for locating all stationary points, namely for reactants, transition states, intermediates, and products. Normal analyses were performed to verify the nature of these stationary points. To confirm the transition state for a given reaction pathway, the minimum energy path from the transition state to both the reactants to products was calculated using the intrinsic reaction path (IRC) following method.[19,20] The continuum conductor-like polarizable continuum model (CPCM, COSMO)[21−23] was used for selected reactions in methanol, tetrahydrofuran, and benzene. Equilibrium constants were calculated using the standard statistical thermodynamic method, and the thermal rate constants for selected reactions were also carried out at the transition state theory (TST) level employing the kinetic module of the web-based Computational Science and Engineering Online (CSE-Online) environment.[24]

Results and Discussion

Model System. Figure 1 shows a schematic drawing of different hydrogen bond complexes used in this study to model the epoxy−amine curing reaction. In particular, we used 2-methoxymethyloxirane to model epoxy, methylamine for primary amine, and propan-2-ol for an alcohol. This model system reasonably describes the first polymerization step in the epoxy−amine curing process in which propan-2-ol represents both a model hydrogen-donating catalyst and a product hydroxyl group and methylamine a curing agent. The next section presents results for possible hydrogen precursor complexes. The actual curing reaction mechanism will be analyzed in detail in the subsequent sections by examining different pathways that involve both the acyclic and cyclic transition states and providing an assessment of their relevance. The influence of solvation on the reaction parameters is also discussed followed by an investigation of solvent effects on secondary versus primary amines.

Hydrogen-Bonding Precursor Complexes. Complexes **1**−**6** (cf. Figure 1) show possible reactant hydrogen complexes between the aliphatic alcohol functional groups, the aliphatic amine functional groups, and the epoxy oxygen. As expected, the OH···O hydrogen bond in **1** is considerably stronger than the NH···N bond in **2**, resulting in a shorter hydrogen bond length and a greater binding energy, as shown in Table 1. The calculated equilibrium constant at 298 K of 3.53 L·mol^{-1} is in good agreement with experimental values (2.45 L·mol^{-1}).[25] Such an agreement validates the accuracy of our theoretical model (level of theory and basis set). Moreover, Table 1 illustrates that OH···N hydrogen bond of **3** shows the strongest hydrogen bonding interaction because OH is a better hydrogen donor than NH and nitrogen is a better hydrogen acceptor (Lewis base) than oxygen. Consistent with such an argument, the NH···O hydrogen bond complexes **4** and **6** have the weakest hydrogen bond energies.

Reaction Mechanism. The epoxy−amine curing reaction can proceed via a number of possible pathways as suggested in the literature, although none has been confirmed by accurate theoretical study. In this study, we examined the three most important pathways, namely the uncatalyzed, self-promoted, and alcohol-catalyzed reaction pathways. The uncatalyzed reaction pathway involves only the epoxy and amine species. Such a reaction pathway is less likely to happen in nature due to the presence of other amine and product alcohol species in the system. However, it serves as a reference system for studying the effects of being self-promoted by other amine species or catalyzing by added alcohol catalyst or the product alcohol species. Each of these reaction pathways can also have two possible routes, namely via an acyclic or a cyclic transition state. Because the differences between acyclic and cyclic TS routes in all three reaction pathways are similar, we present the discussion of the reaction mechanism according to the nature of the TS geometry, i.e., acyclic or cyclic TS route.

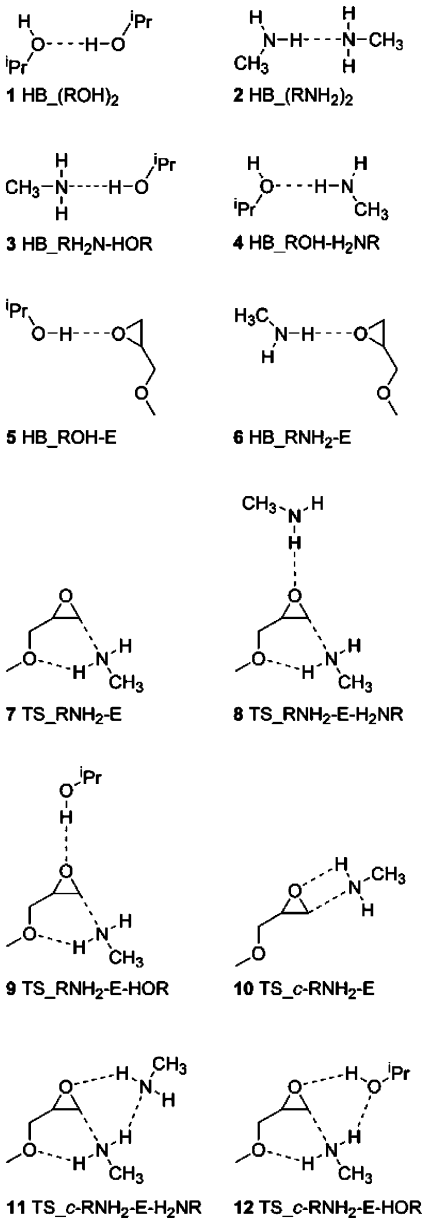

Figure 1. Overview on model complexes. ROH denotes propan-2-ol, RNH_2 methylamine, and E methoxymethyloxirane; HB denotes a hydrogen bond complex, TS denotes acyclic transition state, and TS_*c* for cyclic complex.

Acyclic Transition-State Route. In Table 2, classical barrier heights, $\Delta V^{\ddagger}$, denote the difference in the total electronic energies at the transition states and the corresponding reactants, whereas activation energies, E_a, are obtained from fitting the calculated rate constants to the Arrhenius expression, $Ae^{(-E_a/RT)}$.

Table 1. Hydrogen Complexes[a]

	1 HB_$(ROH)_2$	**2** HB_$(RNH_2)_2$	**3** HB_RH_2N-HOR	**4** HB_ROH-H_2NR	**5** HB_ROH-E	**6** HB_RNH_2-E
d(OH−O) (Å)	1.905				1.94	
d(OH−N) (Å)			1.897			
d(NH−N) (Å)		2.199				
d(NH−O (Å)				2.050		2.219
ΔE_{bind} (kJ × mol^{-1})	−35.2	−19.0	−36.1	−12.7	−31.6	−18.8

[a] d denotes a bond distance (Å) and ΔE_{bind} the energy of the hydrogen bond [kJ × mol^{-1}].

Table 2. Imaginary Frequencies $\nu^{\dagger}$, Selected Optimized Geometrical Parameters of the Transition States along the Acyclic TS Routes, Classical Barrier Heights $\Delta V^{\ddagger}$, Rate Constants $k(T)$ at 300 and 400 K, and Activation Energies E_a of the Uncatalyzed (Figure 2), Self-Promoted (Figure 3), and Alcohol-Catalyzed (Figure 4) Reactions

	7 TS_RNH_2-E (Figure 2)	**8** TS_RNH_2-E−H_2NR (Figure 3)	**9** TS_RNH_2-E-HOR (Figure 4)
$\nu^{\dagger}$ (i·cm^{-1})	374.9	388.8	394.5
d(N1−C1) (Å)	1.858	1.951	2.002
d(H1−O2) (Å)	1.931	1.973	1.994
d(H2−O1) (Å)		1.955	1.712
d(C1−O1) (Å)	2.054	1.994	1.951
d(C2−O1) (Å)	1.347	1.367	1.380
d(C1−C2) (Å)	1.495	1.482	1.476
∠(O1−C2−C1) (deg)	92.4	88.7	86.1
∠(C2−C1−N1) (deg)	113.8	111.6	110.7
$\Delta V^{\ddagger}$ (kJ·mol^{-1})	101.7	76.1	61.6
E_a (kJ·mol^{-1})	109.6	85.1	70.5
k_{fwd} (300 K) (L·mol^{-1}·min^{-1})	7.35×10^{-12}	1.26×10^{-8}	3.06×10^{-6}
k_{fwd} (400 K) (L·mol^{-1}·min^{-1})	4.82×10^{-7}	7.02×10^{-5}	3.92×10^{-3}

Table 3. Imaginary Frequencies $\nu^{\dagger}$, Selected Optimized Geometrical Parameters of the Transition States along the Cyclic TS Routes, Classical Barrier Heights $\Delta V^{\ddagger}$, Rate Constants $k(T)$ at 300 and 400 K, and Activation Energies E_a of the Uncatalyzed (Figure 5), Self-Promoted (Figure 6), and Alcohol-Catalyzed (Figure 7) Reactions

	10 TS_c-RNH_2-E (Figure 5)	**11** TS_c-RNH_2-E-H_2NR (Figure 6)	**12** TS_c-RNH_2-E-HOR (Figure 7)
$\nu^{\dagger}$ (i·cm^{-1})	477.6	414.8	414.9
d(N1−C1) (Å)	2.252	2.217	2.228
d(H2−N2) (Å)		2.039	
d(H2−O2) (Å)			2.019
d(H1−O1) (Å)	1.799	1.976	1.673
d(H3−O1) (Å)		2.151	2.234
d(C1−O1) (Å)	2.079	2.030	2.038
d(C2−O1) (Å)	1.386	1.393	1.400
d(C1−C2) (Å)	1.470	1.467	1.468
∠(O1−C2−C1) (deg)	93.4	90.4	90.5
∠(C2−C1−N1) (deg)	110.9	117.0	118.4
$\Delta V^{\ddagger}$ (kJ·mol^{-1})	181.6	149.3	139.8
E_a (kJ·mol^{-1})	185.2	155.8	145.5
k_{fwd} (300 K) (L·mol^{-1}·min^{-1})	2.45×10^{-24}	3.06×10^{-20}	7.93×10^{-19}
k_{fwd} (400 K) (L·mol^{-1}·min^{-1})	3.20×10^{-16}	1.88×10^{-13}	1.91×10^{-12}

Thus, activation energies also include enthalpic and entropic contributions to the barrier heights.

As the reaction proceeds to the product, the C1−O1 bond is broken and the C1−N1 bond is formed. We used these two "reactive" bond distances in the TS structure to provide information on how close the TS to the reactant (entrance) channel or product (exit) channel. For instance, the smaller C1−O1 and the larger C1−N1 bond distances indicate that the TS is closer to the reactant channel. Comparing the transition state geometries of **7**−**9** indicates that the transition state of the alcohol-catalyzed reaction **9** is closest to the reactant (entrance) channel, while the uncatalyzed reaction **7** is the farthest (i.e., closest to the product channel). This can be seen from the decreases in the C1−O1 bond distances of 2.054, 1.994, and 1.951 Å and the increases in the C1−N1 bond distances of 1.858, 1.951, and 2.002 Å for the uncatalyzed, self-promoted, and alcohol-catalyzed reactions, respectively. This is a charge separation and thus is an endothermic process in the gas phase. According to the Hammond postulate, the more reactant-like characteristics of the transition state will lead to the smaller activation barrier. The order of the calculated activation energies, namely 109.6 kJ·mol^{-1} for the uncatalyzed reaction, 85.1 kJ·mol^{-1} for the self-promoted reaction, and 70.5 kJ·mol^{-1} for the alcohol-catalyzed reaction supports the Hammond postulate. Such an observation can be useful for developing quantitative structure−activity relationships (QSARs) for the epoxy−amine system.

Results presented in Table 2 further suggest that the transition state of the attack of an amine on an epoxy molecule is stabilized by both a hydrogen bond between the amine hydrogen H1 and the ether oxygen O2 and a hydrogen bond between the epoxy oxygen O1 and a hydrogen donor (i.e., H2) that results in lowering the reaction activation barriers. However, because the hydrogen bond between the amine hydrogen H1 and the ether oxygen O2 exists in all three pathways, the determining factor in lowering the activation energy is the hydrogen bond interaction between the epoxy oxygen O1 and a hydrogen donor H2. Our results suggest that the hydrogen bonding with the epoxy

Scheme 2. Comparison of Acyclic and Cyclic Transition State Reaction Pathways.

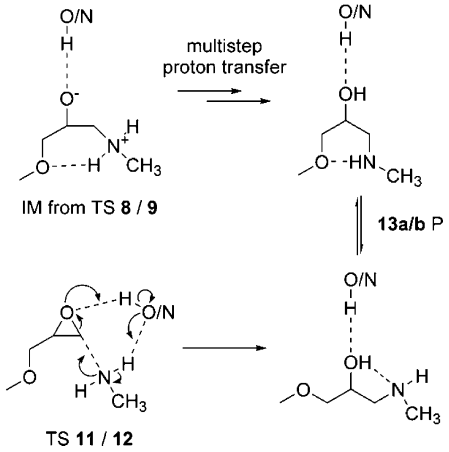

IM is abbreviated for intermediate, and P denotes the product of the reaction

oxygen atom is critical to the reactivity of the epoxy−amine curing reaction. In particular, the alcohol-catalyzed reaction has 14.6 kJ·mol^{-1} lower in the activation energy compared to that of the self-promoted reaction corresponding to its shorter O1−H2 hydrogen bond distance by 0.243 Å.

The small magnitude of the order of 400 cm^{-1} for the imaginary frequencies for all three reaction pathways indicates that the potential energy surfaces of these reactions near the top of the barrier are very flat and thus further supporting that quantum mechanical tunneling would be insignificant and can be ignored. In addition, the activation energies in all cases are higher than the classical barriers by more than 8 kJ·mol^{-1}. This is due to the loss of three translational and three rotational degrees of freedom at the transition state compared to the separated reactants.

Cyclic Transition State Routes. It is well-known that resonance in cyclic transition state structures would potentially provide stabilization effects and lower the activation energy. Possible cyclic transition state routes for epoxy−amine reactions, though, have been suggested previously. They were not confirmed by accurate quantum chemistry calculations.

We found that the reaction pathway via a cyclic transition state exhibits a different mechanism compared to those via an acyclic transition state. In particular, the bond cleavage and bond formation of the epoxy−amine system can occur simultaneously with a hydrogen transfer in a concerted manner, thus directly leading to a product, whereas the pathway via acyclic TS is a stepwise process involving one or more intermediates (IM) as shown in Scheme 2. Although, by comparing the acyclic with the cyclic transition states, the latter exhibit larger steric effects and lack of the ether−oxygen amine−hydrogen bond (H1−O2 in Figures 2−4).

The structure−activity relationship found in the acyclic TS routes described above, namely the later the TS the higher the barrier, is also observed for the cyclic TS routes as shown in Table 3 for TS structures **10** to **12**. In particular, TS structure **10** (Figure 5) represents a four-membered cyclic transition state of the uncatalyzed reaction, TS **11** (Figure 6) for the self-promoted, and TS **12** (Figure 7) for the alcohol-catalyzed reaction, respectively. For the uncatalyzed reaction, IRC calculations confirm that the N1−C1 bond formation, C1−O1 bond cleavage, and O1−H1 bond formation occur simultaneously in a concerted mechanism. This TS geometry also indicates a late transition state relative to both the other cyclic and acyclic

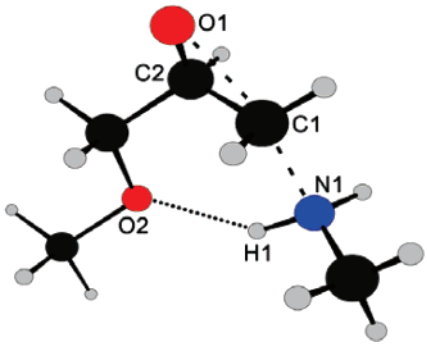

Figure 2. Structure of the transition state of the uncatalyzed pathway (**7** TS_RNH$_2$-E, the corresponding notation in Figure 1 and Table 2). Dark gray is for carbon atoms, light gray for hydrogen, red for oxygen, and blue for nitrogen. Atomic labels are used for the discussion of the geometrical parameters listed in Table 2.

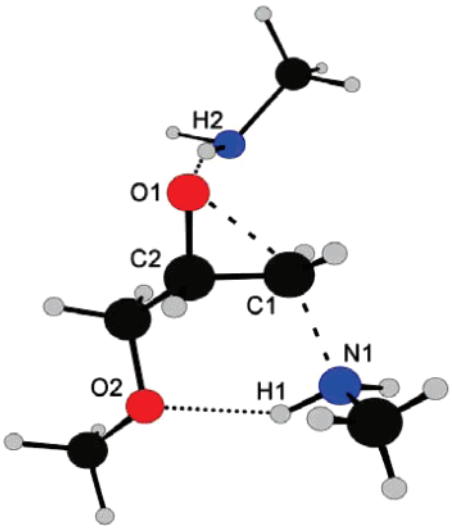

Figure 3. Similar to Figure 2, except for the transition state of the self-promoted pathway (**8** TS_RNH$_2$-E-H$_2$NR, the corresponding notation in Figure 1 and Table 2).

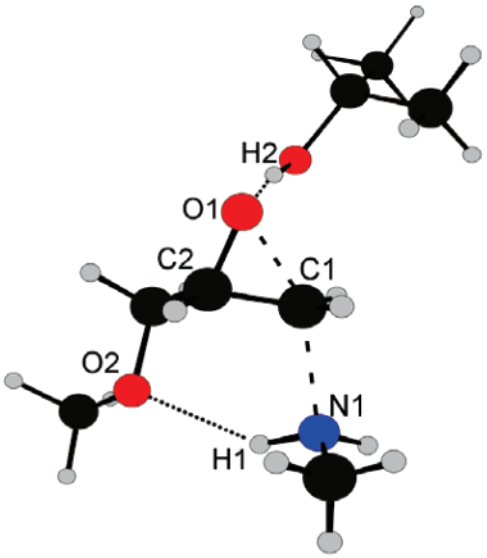

Figure 4. Similar to Figure 2, except for the transition state of the alcohol-catalyzed pathway (**9** TS_RNH$_2$-E-HOR, the corresponding notation in Figure 1 and Table 2).

complexes, together with increased steric crowding, resulting in a high reaction barrier of 181.6 kJ·mol^{-1}, 80 kJ·mol^{-1} higher than that of the corresponding acyclic TS route. In fact, this

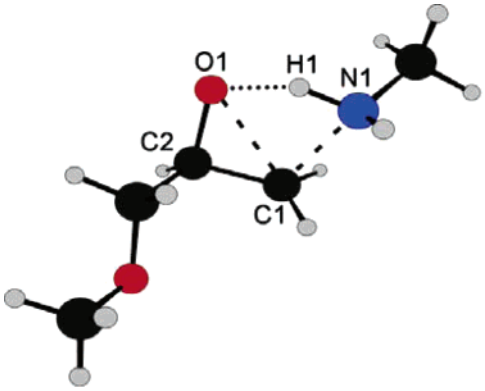

Figure 5. Cyclic transition state for the noncatalyzed pathway **10** TS_*c*-RNH_2-E.

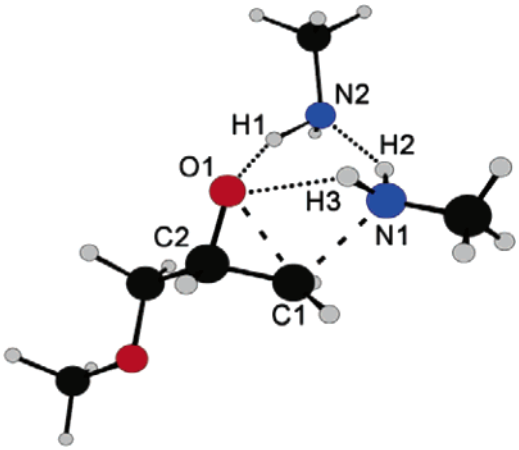

Figure 6. Cyclic transition state for the self-promoted pathway **11** TS_*c*-RNH_2-E-H_2NR.

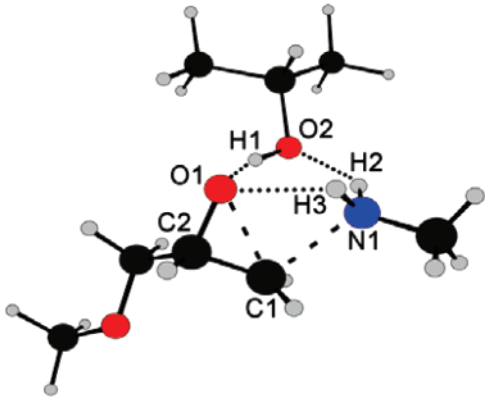

Figure 7. Cyclic transition state for the alcohol-catalyzed pathway **12** TS_*c*-RNH_2-E-HOR.

Scheme 3. In a Six-Membered Cycle, the Actual Reaction Shows as Occurring in a Four-Membered Cycle

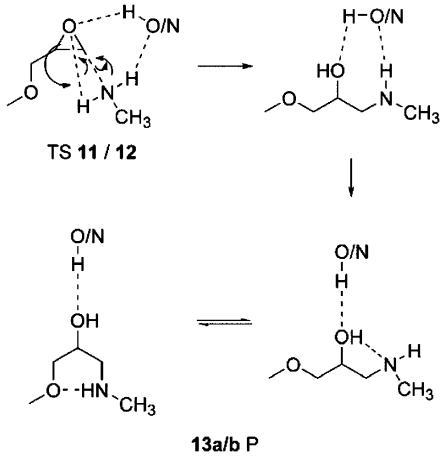

complex was thought to be not reactive previously.[26] For the self-promoted and alcohol-catalyzed pathways, interestingly, IRC results show that the actual reaction, i.e., bond cleavage and formation, preferably occurs in a four-membered ring structure, involving O1, C1, N1, and H3, with a H3−O1 atom distance of 2.151 Å for **11** and 2.234 Å for **12** (cf. Figures 6 and 7, respectively). Scheme 3 illustrates the reaction mechanism and demonstrates that, in this case, the alcohol and second amine molecule, respectively, are merely hydrogen-bonding spectator molecules.

Comparing energetic information for pathways via cyclic and acyclic transition states suggests that possible cyclic reaction pathways play a minor role in the epoxy−amine curing reactions. This is due to the fact that the cyclic arrangement forces an unfavorable nucleophilic *syn*-attack, resulting in steric crowding and hence considerably higher activation barriers, specifically on the order of 80 kJ·mol^{-1} leading to reaction rates several orders of magnitude lower than those via acyclic TS routes. In addition to high classical barriers, the activation entropy argues against the formation of such cyclic TS complexes. Note that it is possible to form TS cyclic routes that involve a larger number of spectator (amine and/or alcohol) molecules as discussed by Okumoto and Yamabe.[27] However, the polymer matrix and thermal motions would argue against the contribution of such cyclic TS routes in the realistic environment.

Solvent Effects. Solvent effects on geometries of the stationary points, activation energy, and reaction rates of the alcohol-catalyzed reaction via the acyclic TS route, the lowest energy route, were studied using the CPCM continuum model for three different solvents; benzene represents nonpolar solvents, tet-

Table 4. Transition State Properties for the Catalyzed Reaction via the Acyclic TS Route (9 TS_RNH_2-E-HOR as in Figure 4) in Different Solvents

	gas phase	CPCM benzene	CPCM tetrahydrofuran	CPCM methanol
ϵ_r	1	2.247	7.58	32.63
$\nu^{\dagger}$ (i·cm^{-1})	394.5	440.0	468.5	482.8
d(N1−C1) (Å)	2.002	2.077	2.129	2.146
d(H1−O2) (Å)	1.994	2.082	2.152	2.181
d(H2−O1) (Å)	1.712	1.711	1.734	1.733
d(C1−O1) (Å)	1.951	1.893	1.857	1.845
d(C2−O1) (Å)	1.380	1.392	1.400	1.403
d(C1−C2) (Å)	1.476	1.468	1.462	1.461
∠(O1−C2−C1) (deg)	86.1	82.8	80.9	80.2
∠(C2−C1−N1) (deg)	110.7	109.4	108.3	108.1
$\Delta V^{\ddagger}$ (kJ·mol^{-1})	61.6	55.3	52.2	51.0
E_a (kJ·mol^{-1})	70.5	64.2	61.0	59.0
k_{fwd} (300 K) (L·mol^{-1}·min^{-1})	3.06×10^{-6}	1.43×10^{-4}	4.57×10^{-4}	5.55×10^{-3}
k_{fwd} (400 K) (L·mol^{-1}·min^{-1})	3.92×10^{-3}	9.82×10^{-2}	2.30×10^{-1}	2.28

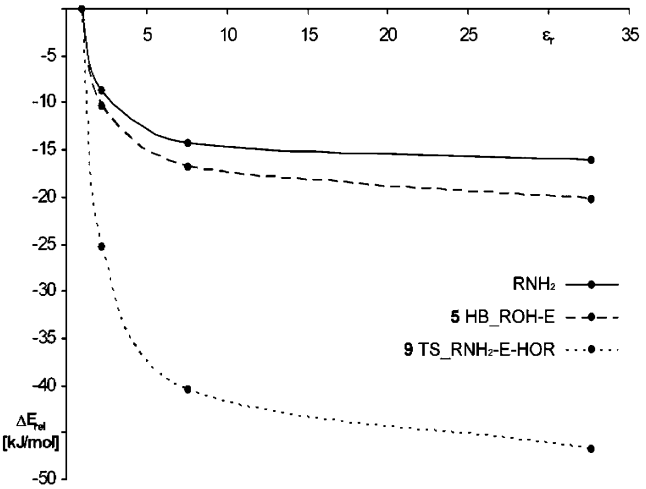

Figure 8. Solvation free energies of the reactant species methylamine (A), epoxy-propan-2-ol complex **5** (HB_ROH-E), and the resulting transition state **9** (TS_RNH_2-E-HOR) as functions of the solvent polarity represented by its dielectric constant.

rahydrofuran slightly polar and methanol polar solvents. Note that the specific hydrogen bond effects are included explicitly in the complex TS **9**. Table 4 indicates that increasing solvent polarity causes an earlier transition state, which has already been discussed in the reaction mechanism section and recognized as the main indicator for lowering the activation barrier. Polar solvent solvates the charge-separated product $O^-\cdots N^+$, making it more exothermic. According to the Hammond postulate, this will lead to more reactant-like TS and lower the activation barrier.

The effect of solvent polarity is shown in Figure 8. It displays the solvation free energies of reactants and TS as functions of the solvent dielectric constant ϵ_r. The results indicate that increasing the solvent polarity will solvate the TS more than the reactants and thus lower the activation energy. The chart shows that most of the effects can be achieved with moderate solvent polarity. These results are consistent with earlier studies on this topic.[28]

Comparisons with Experimental Data. From experimental studies, Mijovic reported rate constants on the order of between 10^{-3} and 10^{-2} at 393 K (120 °C) for both primary and secondary amines for the alcohol-catalyzed reaction of phenylglycidyl ether and aniline.[8,29] Matejka obtained the same order of magnitude for the system diglycidylaniline−aniline at 373 K (100 °C).[30,31] Comparing these values with the calculated rate constant of 3.9×10^{-3} and 9.82×10^{-2} at 400 K for the alcohol-catalyzed reaction in the gas phase and in nonpolar solvent, respectively, it may be justified to state that the computational methodology used in this study is adequate for obtaining kinetic information from DFT methods.

The calculated activation energies E_a can be compared directly to experimental values. Paz-Abuin reported the activation energy of 52.8 kJ·mol^{-1} for the alcohol-catalyzed reaction of diglycidyl ether of bisphenol A (DGEBA) with 1,3-bis(aminomethyl)-cyclohexane (1,3 BAC) and 62.3 kJ·mol^{-1} for the uncatalyzed one.[12] Blanco found the activation energies of 64.9 kJ·mol^{-1} and 41.4 kJ·mol^{-1} for DGEBA with *p*-methylaniline and toluidine, respectively.[10] Vinnik reported a value of 51 kJ·mol^{-1} for the catalyzed reaction of phenylglycidyl ether (PGE) with aniline.[32] The calculated activation energies for the most favorable pathway, i.e., the alcohol-catalyzed reaction via the acyclic TS structure route, as shown in Table 4 for several solvent environments, are in fact within the experimental range.

Scheme 4. Schematic Illustration of the Mechanism of the Initial Stage of the Epoxy−Amine Polymerization

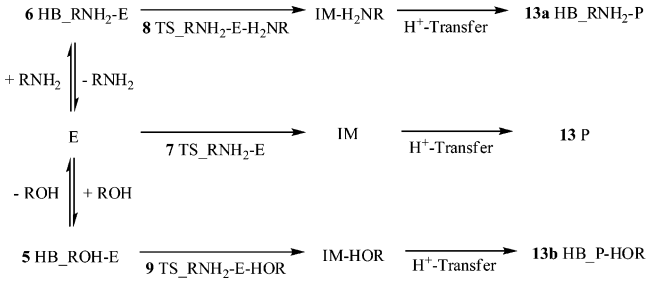

Overall Mechanism. To investigate the relative importance of different pathways from the epoxy to the addition product **13**, e.g., uncatalyzed, catalyzed by alcohol, and self-promoted by amine, we examine the overall mechanism consisting of all important pathways as described in Scheme 4. A comparison between the uncatalyzed pathway via the TS complex **7** with the alcohol-catalyzed pathway via the TS complex **9**, as illustrated in the middle and lower row of Scheme 4, leads to the suggestion that adding a small amount of alcohol to the epoxy−amine mixture would accelerate the overall curing reaction rate, with a greater impact at lower temperatures. The same statement is also true for the self-promoted reaction pathway, which is illustrated in the upper row of Scheme 4 but to a lesser extent. However, it is important to point out that, although the activation energies for both the catalyzed and self-promoted reactions are lower than that of the uncatalyzed pathway, the formation constants K_c for the hydrogen precursor complexes for these pathways must also be taken into account. Complex **6**, which leads to the transition state complex **8**, is less likely to form than complex **5** by almost 2 orders of magnitude (estimated from the difference in the binding energies). From these arguments, it is possible that the uncatalyzed pathway (via complex **7**) and the self-promoted pathway (via complex **6** leading to complex **8**) may be competing in the absence of any added catalyst, whereas the alcohol-catalyzed pathway (via complex **5** leading complex **9**) is supposed to be the most probable pathway whenever an alcohol catalyst is present or the product alcohol species can participate in the reaction.

Primary versus Secondary Amines. There exists an interesting fact about the ratio of rate constants for primary and secondary amines. Most studies agreed that the ratio (secondary/primary) is somewhere between 0.5 (e.g., Horie kinetic model[7]) and unity.[33] All suggested that the major reasons for the decrease in the rate is due to steric effects caused by bulky substituents and electronic effects resulting from the differences in the nitrogen atom of the primary and secondary amines.

In this study, we used dimethylamine to model secondary amine and assumed that the alcohol-catalyzed reaction pathway dominates the kinetics of the overall reaction. In contrast to the earlier accepted fact, the data of Table 4 suggests that solvent effects are the key reason for secondary amines to react slower than primary species. The steric and electronic effects are included in the gas-phase reaction by using complex TS **14** as a model secondary amine. The barrier height in gas phase is lower for secondary amines. This result suggests that secondary amines would react faster than primary amines rather than slower as observed experimentally. Such a contradiction suggests that steric and electronic effects are not the reason for the experimental observation as suggested previously. When solvent effects are included by using methanol as a model, consistent with experimental observation, is obtained. Figure 9 depicts the

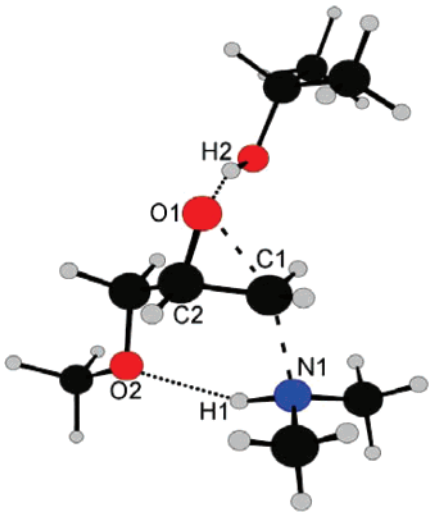

Figure 9. Transition state for the alcohol-catalyzed pathway of a secondary amine **14** TS_R_2NH-E-HOR.

transition state, which shows that steric effects play a minor role and the substitution effect is rather small.[34] The calculated ratio of rate constants is much smaller than reported in experiments. This is due to the fact that actual bulk environment in a real cure reaction would have much less solvent polarity than methanol as modeled here. The present results, nevertheless, provide a correct trend.

Conclusions

The mechanism of the epoxy−amine curing reaction has been examined at the molecular level by using a system of three model compounds, namely 2-methoxymethyloxirane to model epoxy, methylamine for primary amine, and propan-2-ol for an alcohol. Potential energy surfaces, along different reaction pathways, were calculated at the B3LYP/6-31G(d,p) level of theory. Equilibrium of hydrogen bond precursor complexes and thermal rate constants for different pathways were also computed.

The polymerization reaction can be divided into noncatalytic, self-promoted by amine, and alcohol-catalyzed types, with reaction pathways proceeding via either cyclic and acyclic transition state routes. The acyclic alcohol-catalyzed pathway exhibits the lowest activation barrier and consequently is the most favorable of all examined pathways. It is noteworthy that the curing reaction generates a hydroxyl group from the epoxy oxygen so that the polymerization is accelerated with proceeding conversion, and thus the alcohol-catalyzed pathway always dominates in later stages of conversion. In the absence of a catalyst, the curing reaction may proceed via both the acyclic noncatalytic and self-promoted pathways, the latter exhibiting the faster reaction rate. These pathways are only important at early stages of conversion due to the possible auto-acceleration of the reaction by the product hydroxyl-groups.

Although pathways involving cyclic transition states have been suggested as more favorable, the results indicate that they are not important for the curing reaction because of their high activation barriers due to steric crowding and entropy of activation.

Investigations on the influence of solvent effects from the bulk phase have also been made using a continuum solvation model. Solvent effects were found to lower the activation energy and are more profound with an increase in solvent polarity.

Finally, the study of the differences in the reactivity of primary and secondary amine yields interesting results. Steric crowding and electronic effects were thought previously to be the main influence on the observed slower rate in the secondary amine. The present results indicate that these yield the opposite effect, namely the secondary amine reacts faster. Solvent effects are the key factor for the slower rate of secondary amine.

Acknowledgment. This work is supported in part by Dow Chemical company. J.E. thanks the DAAD (German Academic Exchange Service) for providing a scholarship for the exchange between the Chemistry Departments of the Technische Universität Braunschweig, Germany, and the University of Utah. The computational resources for this project have been provided by the National Institutes of Health (grant no. NCRR 1 S10 RR17214-01) on the Arches Metacluster, administered by the University of Utah Center for High Performance Computing.

References and Notes

(1) Harper, C. A. In *Handbook of Plastics, Elastomers and Composites*, 2nd ed.; McGraw-Hill: New York, **1992**; pp 10−55.
(2) Sometimes tertiary amines are included in discussions even though they are not considered as curing agent.
(3) Narracott, E. S. *Br. Plast. Moulded Prod. Trader* **1953**, *26*, 120−122.
(4) Chapman, N. B.; Isaacs, N. S.; Parker, R. E. *J. Chem. Soc.* **1959**, 1925−1934.
(5) Shechter, L.; Wynstra, J.; Kurkjy, R. P. *J. Ind. Eng. Chem.* **1956**, *48*, 94−97.
(6) Smith, I. T. *Polymer* **1961**, *2*, 95−108.
(7) Horie, K.; Hiura, H.; Sawada, M.; Mita, I.; Kambe, H. *J. Polym. Sci., Part A-1: Polym. Chem.* **1970**, *8*, 1357−1372.
(8) Mijovic, J.; Fishbain, A.; Wijaya, J. *Macromolecules* **1992**, *25*, 979−985.
(9) Cole, K. C. *Macromolecules* **1991**, *24*, 3093−3097.
(10) Blanco, J. M.; Corcuera, M. A.; Riccardi, C. C.; Mondragon, I. *Polymer* **2005**, *46*, 7989−8000.
(11) For example, an approach similar to the two-fluid model for glassy state transition: Vinnik, R. M.; Roznyatovsky, V. A. *J. Therm. Anal. Calorim.* **2003**, *73*, 807−817.
(12) Paz-Abuin, S.; Pellin, M. P.; Paz-Pazos, M.; Lopez-Quintela, A. *Polymer* **1997**, *38*, 3795−3804.
(13) Zvetkov, V. L. *Macromol. Chem. Phys.* **2002**, *203*, 467−476.
(14) Rozenberg, B. A. *Adv. Polym. Sci.* **1985**, *75*, 113−165.
(15) Noyori hydrogenation: Noyori, R.; Hashiguchi, S. *Acc. Chem. Res.* **1997**, *30*, 97−102.
(16) Meerwein−Ponndorf−Verley reaction: Meerwein, H.; Schmidt, R. *Justus. Liebigs. Ann. Chem.* **1925**, *444*, 221−238; Ponndorf, W. *Angew. Chem.* **1926**, *39*, 138−143; Verley, A. *Bull. Soc. Chim. Fr.* **1925**, *37*, 537−542.
(17) Frisch, M. J.; Trucks, G. W.; Schlegel, H. B.; Scuseria, G. E.; Robb, M. A.; Cheeseman, J. R.; Montgomery, J. A., Jr.; Vreven, T.; Kudin, K. N.; Burant, J. C.; Millam, J. M.; Iyengar, S. S.; Tomasi, J.; Barone, V.; Mennucci, B.; Cossi, M.; Scalmani, G.; Rega, N.; Petersson, G. A.; Nakatsuji, H.; Hada, M.; Ehara, M.; Toyota, K.; Fukuda, R.; Hasegawa, J.; Ishida, M.; Nakajima, T.; Honda, Y.; Kitao, O.; Nakai, H.; Klene, M.; Li, X.; Knox, J. E.; Hratchian, H. P.; Cross, J. B.; Bakken, V.; Adamo, C.; Jaramillo, J.; Gomperts, R.; Stratmann, R. E.; Yazyev, O.; Austin, A. J.; Cammi, R.; Pomelli, C.; Ochterski, J. W.; Ayala, P. Y.; Morokuma, K.; Voth, G. A.; Salvador, P.; Dannenberg, J. J.; Zakrzewski, V. G.; Dapprich, S.; Daniels, A. D.; Strain, M. C.; Farkas, O.; Malick, D. K.; Rabuck, A. D.; Raghavachari, K.; Foresman, J. B.; Ortiz, J. V.; Cui, Q.; Baboul, A. G.; Clifford, S.; Cioslowski, J.; Stefanov, B. B.; Liu, G.; Liashenko, A.; Piskorz, P.; Komaromi, I.; Martin, R. L.; Fox, D. J.; Keith, T.; Al-Laham, M. A.; Peng, C. Y.; Nanayakkara, A.; Challacombe, M.; Gill, P. M. W.; Johnson, B.; Chen, W.; Wong, M. W.; Gonzalez, C.; Pople, J. A. *Gaussian 03*, revision A.1; Gaussian, Inc.: Pittsburgh, PA, 2003.
(18) Becke, A. D. *J. Chem. Phys.* **1993**, *98*, 5648−5652.
(19) Gonzalez, C.; Schlegel, H. B. *J. Chem. Phys.* **1989**, *90*, 2154−2161.
(20) Gonzalez, C.; Schlegel, H. B. *J. Phys. Chem.* **1990**, *94*, 5523−5527.
(21) Barone, V.; Cossi, M. *J. Phys. Chem. A* **1998**, *102*, 1995−2001.
(22) Cossi, M.; Rega, N.; Scalmani, G.; Barone, V. *J. Comput. Chem.* **2003**, *24*, 669−681.
(23) Cammi, R.; Mennucci, B.; Tomasi, J. *J. Phys. Chem. A* **2000**, *104*, 5631−5637.
(24) Truong, T. N.; Nayak, M.; Huynh, H. H.; Cook, T.; Mahajan, P.; Tran, L.-T. T.; Bharath, J.; Jain, S.; Pham, H. B.; Boonyasiriwat, C.; Nguyen,

N.; Andersen, E.; Kim, Y.; Choe, S.; Choi, J.; Cheatham, T. E., III; Facelli, J. C. *J. Chem. Inf. Model.* **2006**, *46*, 971.
(25) References cited in Rozenberg, B. A. *Adv. Polym. Sci.* **1985**, *75*, 113−165.
(26) Vinnik, R. M.; Roznyatovsky, V. A. *J. Therm. Anal. Calorim.* **2003**, *73*, 819−826.
(27) Okumoto, S.; Yamabe, S. *J. Comput. Chem.* **2003**, *24*, 244−253.
(28) Vedenyapina, N. S.; Kuznetsova, V. P.; Ivanov, V. V.; Zelenetskii, A. N.; Rakova, G. V.; Plokhotskaya, L. A.; Ponomarenko, A. T.; Shevchenko, V. G.; Enkolopyan, N. S. *Izv. Akad. Nauk SSSR, Ser. Khim.* **1976**, *9*, 1956−1962.
(29) Mijovic, J.; Wijaya, J. *Macromolecules* **1992**, *27*, 7589−7600.
(30) Matejka, L.; Dusek, R. *Macromolecules* **1989**, *22*, 2911−2917.
(31) It is important to mention that the alcohol-catalyzed reaction is assumed as a thermomolecular reaction resulting in a third-order rate constant ($L^2 \cdot mol^{-2} \cdot min^{-1}$). In contrast, in this study it is assumed that the epoxy and alcohol molecules react in a pre-equilibrium (cf. Scheme 4) that results in a second-order rate constant ($L \cdot mol^{-1} \cdot min^{-1}$).
(32) Vinnik, R. M.; Roznyatovsky, V. A. *J. Therm. Anal. Calorim.* **2004**, *76*, 285−293.
(33) For example, Grillet, A. C.; Galy, J.; Pascault, J. P.; Bardin, J. *Polymer* **1989**, *30*, 2094−2103.
(34) As an indicator: $pK_a = 10.66$ for methylamine and $pK_a = 10.73$ for dimethylamine.

MA070423M